



HAL
open science

Coordinatively Unsaturated Amidotitanocene Cations with Inverted σ and π Bond Strengths: Controlled Release of Aminyl Radicals and Hydrogenation/Dehydrogenation Catalysis

Adrien Thomas Normand, Quentin Bonnin, Tereza Edlová, E. Daiann Sosa Carrizo, Paul Fleurat-Lessard, H el ene Cattey, Philippe Richard, Pierre Le Gendre, St ephane Brand es

► To cite this version:

Adrien Thomas Normand, Quentin Bonnin, Tereza Edlov a, E. Daiann Sosa Carrizo, Paul Fleurat-Lessard, et al.. Coordinatively Unsaturated Amidotitanocene Cations with Inverted σ and π Bond Strengths: Controlled Release of Aminyl Radicals and Hydrogenation/Dehydrogenation Catalysis. Chemistry - A European Journal, 2021, 10.1002/chem.202103487 . hal-03389721

HAL Id: hal-03389721

<https://hal.science/hal-03389721>

Submitted on 21 Oct 2021

HAL is a multi-disciplinary open access archive for the deposit and dissemination of scientific research documents, whether they are published or not. The documents may come from teaching and research institutions in France or abroad, or from public or private research centers.

L'archive ouverte pluridisciplinaire **HAL**, est destin ee au d ep ot et  a la diffusion de documents scientifiques de niveau recherche, publi es ou non,  emanant des  tablissements d'enseignement et de recherche fran ais ou  trangers, des laboratoires publics ou priv es.

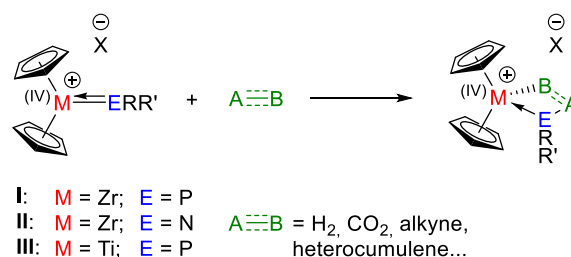
Coordinatively Unsaturated Amidotitanocene Cations with Inverted σ and π Bond Strengths: Controlled Release of Aminyl Radicals and Hydrogenation/Dehydrogenation Catalysis

Quentin Bonnin,^{[+][a]} Tereza Edlová,^[+] E. Daiann Sosa Carrizo,^{[+]*} Paul Fleurat-Lessard, Stéphane Brandès, Hélène Cattey, Philippe Richard, Pierre Le Gendre* and Adrien T. Normand*

Abstract: Cationic amidotitanocene complexes $[\text{Cp}_2\text{Ti}(\text{NPhAr})][\text{B}(\text{C}_6\text{F}_5)_4]$ ($\text{Cp} = \eta^5\text{-C}_5\text{H}_5$; $\text{Ar} = \text{phenyl}$ (**1a**), p -tolyl (**1b**), p -anisyl (**1c**)) were isolated. The bonding situation was studied by Density Functional Theory using EDA-NOCV (Energy Decomposition Analysis with Natural Orbitals for Chemical Valence). The polar Ti-N bond in **1a-c** features an unusual inversion of σ and π bond strengths responsible for the balance between stability and reactivity in these coordinatively unsaturated species. In solution, **1a-c** undergo photolytic Ti-N cleavage to release Ti(III) species and aminyl radicals $\bullet\text{NPhAr}$. Reaction of **1b** with H_3BNHMe_2 results in fast homolytic Ti-N cleavage to give $[\text{Cp}_2\text{Ti}(\text{H}_3\text{BNHMe}_2)][\text{B}(\text{C}_6\text{F}_5)_4]$ (**3**). **1a-c** are highly active precatalysts in olefin hydrogenation and silanes/amines cross-dehydrogenative coupling, whilst **3** efficiently catalyzes amine-borane dehydrogenation. The mechanism of olefin hydrogenation was studied by DFT and the cooperative H_2 activation key step was disclosed using the Activation Strain Model (ASM).

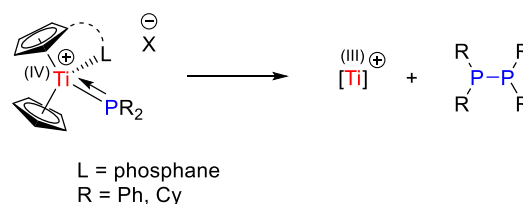
Introduction

Metallocene alkyl cations Cp_2MR^+ ($\text{M} = \text{Ti, Zr, Hf}$) have attracted considerable attention during the last decades as active homogeneous catalysts for olefin polymerization.^[1] Recently, we set out to explore the reactivity of analogous systems in which the M-alkyl substituent is replaced by a phosphido or amido ligand.^[2] The presence of a lone pair of electrons next to an electrophilic metal is ideally suited for the cooperative activation of polar(izable) bonds (Scheme 1).^[3] We previously reported on phosphido- and amidozirconocene cations (**I** and **II**), and we established that these species are useful as hydrogenation catalysts and as Frustrated Lewis Pair (FLP) precursors.^[2a] By contrast, phosphidotitanocene cations (**III**) are much more difficult to tame, due to facile Ti-P bond homolysis. Thus, thermodynamically more stable mixtures of diphosphanes — after phosphinyl radical dimerization — and Ti(III) species are usually obtained as end products.^[4]



Scheme 1. Small molecule activation with group IV amido- and phosphidometallocene cations.

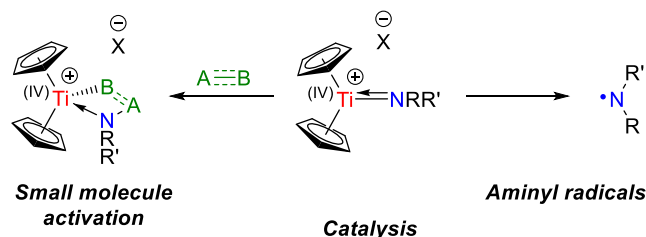
Nevertheless, coordinative saturation by phosphane donors (Scheme 2) mitigates the redox-lability of these otherwise elusive species, so that the release of phosphinyl radicals can be controlled to some extent.^[2a]



Scheme 2. Ti-P bond homolysis and phosphinyl radical recombination in phosphidotitanocene cations.

In light of the commonness of titanium amide precatalysts,^[5] we surmised that amidotitanocene cations (Scheme 3) should display enhanced stability compared to **III**. Consequently, they should be able to release aminyl radicals in a more controlled manner — an intriguing prospect, given the prevalence of aminyl radicals as key intermediates / catalysts in the synthesis of nitrogen-containing organic compounds.^[6] On the other hand, we also expected similar reactivity towards small molecules as that displayed by complexes **I-III**.

Reactivity / Stability ?



Scheme 3. Amidotitanocene cations (this work).

[a] Dr Q. Bonnin, T. Edlová, Dr E. D. Sosa Carrizo, Dr H. Cattey, Dr P. Richard, Prof Dr P. Fleurat-Lessard, Prof Dr P. Le Gendre, Dr A. T. Normand.
 Institut de Chimie Moléculaire de L'Université de Bourgogne (ICMUB), Université de Bourgogne, 9 avenue Alain Savary, 21000 Dijon (FR)

[+]
 Co-first authors
 E-mail: eric-daiann.sosa-carrizo@u-bourgogne.fr; pierre.le-gendre@u-bourgogne.fr; adrien.normand@u-bourgogne.fr.

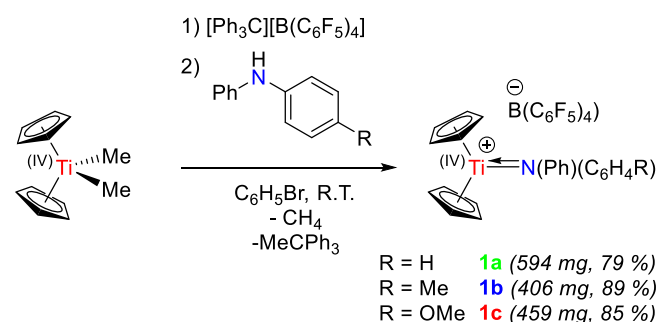
Supporting information for this article is given via a link at the end of the document

We now report our investigations into the synthesis of cationic amidotitanocene complexes, their stability / reactivity and their catalytic behavior. We have found that these complexes i) efficiently catalyze hydrogenation and dehydrogenation reactions; ii) undergo Ti-N bond homolysis, a process which can be triggered either by irradiation with visible light or by the addition of neutral donors. These experimental results are complemented with density functional theory (DFT) calculations to elucidate the bonding situation in amidotitanocene cations and the observed reactivity / catalytic activity.

Results and Discussion

Synthesis and bonding

Complexes **1a-c** were synthesized by protonolysis of $[\text{Cp}_2\text{TiMe}][\text{B}(\text{C}_6\text{F}_5)_4]$ (generated in situ) with a diarylamine (Scheme 4). These compounds could be isolated as air- and light-sensitive dark green powders in good yields (79-89%). They are moderately stable in solution (decomposition is observed over a few hours in CD_2Cl_2), but they can be stored for weeks under argon below -15°C . They were characterized by multinuclear NMR spectroscopy, UV-vis and IR spectroscopy, and elemental analysis.



Scheme 4. Synthesis of complexes **1a-c**.

Single crystals of **1b** suitable for X-ray diffraction were obtained by slow diffusion of heptane into a chlorobenzene solution of **1b** (Figure 1, left). The molecular structure of **1b** shows a trigonal-planar Ti cation bound to two Cp and one amido ligands ($\Sigma\alpha(\text{Ti}) = 359.96(11)^\circ$). Intriguingly, no additional interaction can be found; this is in stark contrast with amidozirconocene cations **II**, which obviate coordinative unsaturation by interacting with the $\text{MeB}(\text{C}_6\text{F}_5)_3^-$ anion or an aromatic ring on the amido ligand.^[2a] The N atom features a trigonal planar geometry ($\Sigma\alpha(\text{N}) = 360.0(3)^\circ$) and the amido ligand forms a dihedral angle (φ) of $47.42(10)^\circ$ with the σ -ligand plane (Figure 1, right). This orientation results from a compromise between i) the minimization of unfavorable steric interactions between the aryl groups of the amido ligand and the Cp rings;^[7] ii) the maximization of p_π - d_π overlap between N and the metal.^[8] The Ti-N distance ($1.9792(19) \text{ \AA}$) is markedly inferior to the sum of covalent radii of Ti and N ($2.31 \pm 0.09 \text{ \AA}$),^[9] suggestive of partial double bond character (vide infra).

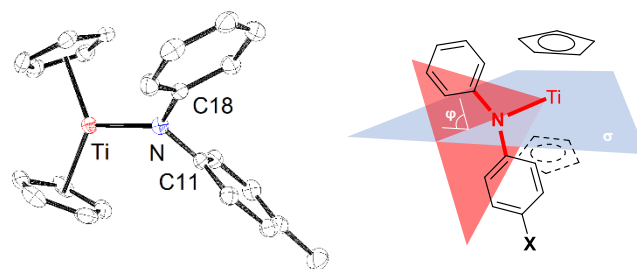


Figure 1. (left) ORTEP view of **1b**. H atoms and the $\text{B}(\text{C}_6\text{F}_5)_4^-$ anion are omitted for clarity; (right) the dihedral angle φ is the angle between the " σ " plane bisecting the two Cp least square plane and the (Ti,N,C11,C18) least squares plane.

The ^1H NMR spectra of diamagnetic complexes **1a-c** (600 MHz, $\text{C}_6\text{D}_5\text{Br}$, 298 K) are trivial, except for one remarkable feature: the signals of the aromatic ortho protons are markedly shifted upfield from the aromatic resonance range ($5.43 \leq \delta \leq 5.75 \text{ ppm}$). We tentatively ascribe this shielding to the coordinative unsaturation of Ti, which allows the ortho protons to enter the magnetic anisotropy cone of the Cp rings. Agostic interactions are precluded, based on the observed free rotation of the amido ligand around the Ti-N axis on the one hand, and the absence of evidence for such interactions in the X-ray structure of **1b** on the other hand.

The $^{15}\text{N}, ^1\text{H}$ HMBC NMR spectra of complexes **1a-c** show a signal ($\delta \approx -30 \text{ ppm}$) which is shifted considerably downfield compared to that of the parent diphenylamine ($\delta = -288.5 \text{ ppm}$ in DMSO).^[10] This is consistent with the behavior of **I-III**, and more generally with that of d^0 alkylidene complexes,^[11] which are isoelectronic to group IV amido- and phosphidometallocene cations.

The UV-visible spectra of complexes **1a-c** displayed in Figure 2 show distinctive local maxima around 400 nm ($\epsilon \approx 10^4 \text{ M}^{-1}\cdot\text{cm}^{-1}$) which — along with the weaker band tailing into the IR region — is responsible for the green color of complexes **1a-c**.

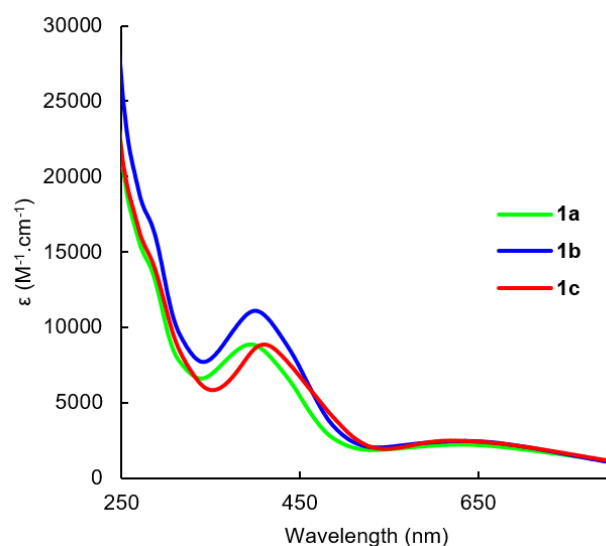


Figure 2. UV-vis spectra of **1a-c** in CH_2Cl_2 .

Table 1. EDA results for **1a**^[a]

Structure	1a ^A	1a ^B	1a ^C	1a ^D	1a ^B
Fragments	Cp ₂ Ti(T)	Cp ₂ Ti(S)	Cp ₂ Ti ²⁺ (S)	Cp ₂ Ti ⁺ (D)	Cp ₂ Ti ⁺ (D)
	NPh ₂ ⁺ (T)	NPh ₂ ⁺ (S)	NPh ₂ ⁺ (S)	NPh ₂ (D)(σ)	NPh ₂ (D)(π)
ΔE_{int}	-133.3	-134.2	-298.9	-106.0	-79.8
ΔE_{Pauli}	120.37	165.9	133.1	113.0	131.1
ΔE_{elstat}	-65.8	-100.0	-263.3	-75.2	-101.0
$\Delta E_{\text{Dispersion}}$	-19.7	-19.7	-19.7	-19.7	-19.7
ΔE_{Orb}	-168.2	-180.5	-148.1	-124.1	-90.2
$\Delta E_{\text{Orb}-\sigma}$	-84.3	-14.9	-50.7	-80.6	-28.4
$\Delta E_{\text{Orb}-\pi}$	-69.0	-156.0	-48.7	-21.2	-42.3
% ΔE_{elstat}	25	33	61	34	47
% ΔE_{Orb}	66	60	34	56	42
% $\Delta E_{\text{Dispersion}}$	7	6	4	8	9

[a]: energy contributions in kcal.mol⁻¹. (S): singlet; (D): doublet; (T): triplet.

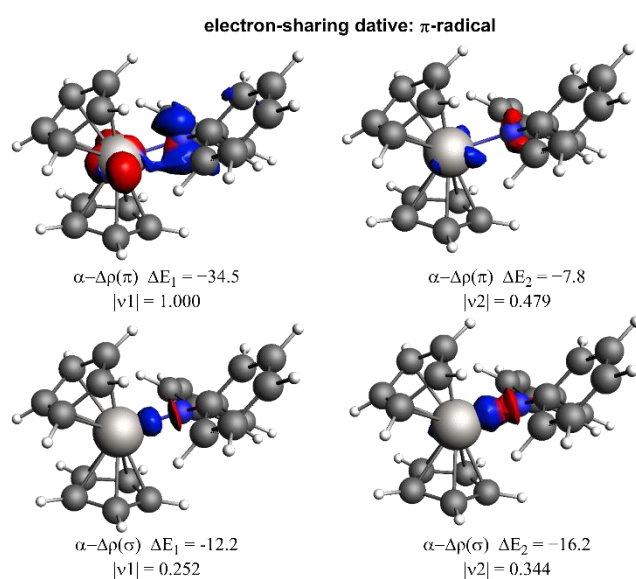


Figure 5. Plot of the deformation densities ($\Delta\rho$) and associated stabilization energies $\Delta E(p)$ for **1a**^D (π -radical). Charge flow: red→ blue. Eigenvalues $|v|$ indicate the relative size of the charge flow.

The main EDA results are summarized in Table 1.^[21] It appears that **1a**^D (π radical) is the preferred Lewis structure: indeed, it displays the lowest absolute value of ΔE_{orb} (-90.2 kcal.mol⁻¹), which means that the electronic structures of the corresponding fragments (doublet Cp₂Ti⁺ and doublet NPh₂ π -radical) are the least altered by the interaction to give **1a**^D.^[22] Interestingly, the NOCV analysis reveals that the (dative) σ contribution to ΔE_{orb} is smaller than the (electron-sharing) π contribution (-28.4 vs -42.3 kcal.mol⁻¹); reversal of σ and π bonding strengths, although rare, has been noted elsewhere in the case of a bicyclic tetrasilane.^[23] The Ti=N double-bond character is likely an important factor contributing to the remarkable stability of amidotitanocene cations in the ground state; however this stability is precarious, since rotation of the amido ligand around the Ti-N bond (as observed

by ¹H NMR spectroscopy) puts the major π component under constant threat of collapse.

Figure 5 shows the α and β contributions to the deformation densities ($\Delta\rho$) of the pairwise orbital interactions in **1a**^D (π -radical). The considerable Cp₂Ti⁺→NPh₂ charge flow ($|v1| = 1.000$ e) results in a net flow 0.521e in the Ti→N direction, consistent with the oxidation of the d¹ Cp₂Ti⁺ fragment upon bond formation. On the other hand, the net Cp₂Ti⁺←NPh₂ charge flow corresponding to the Ti←N dative bond amounts to 0.596e. A similar situation was noted elsewhere for the diatomic molecule BF.^[17c]

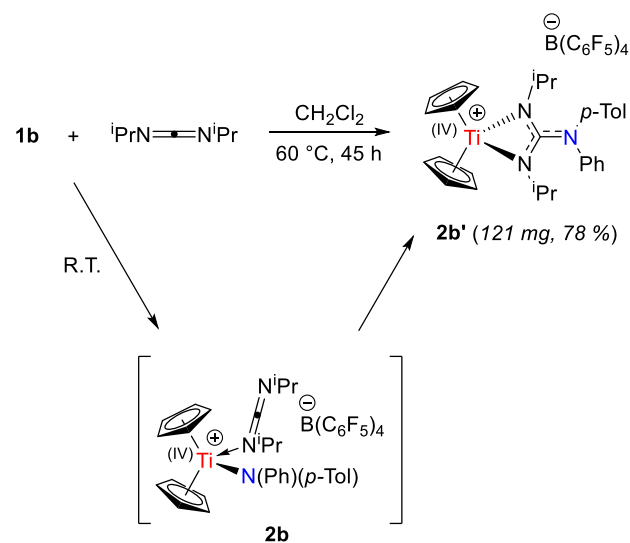
Reactivity

We tested the reactivity of complex **1b** against a wide range of substrates (see the Supporting Information), including H₂, CO₂, diphenylacetylene and chalcone, which were previously shown to react with **I-III**. In most cases, complex and intractable mixtures were obtained.

A notable exception was diisopropylcarbodiimide (DIC), which afforded DIC adduct **2b** at room temperature, and guanidinate complex **2b'** after heating at 60 °C for 45 h in CH₂Cl₂ (Scheme 6). The DIC adduct **2b** was unstable and evolved towards **2b'** over time in CD₂Cl₂; nevertheless it could be characterized by single crystal X-ray diffraction analysis.

The X-ray structure of **2b** (Figure 6) shows the carbodiimide ligand coordinated in η^1 -fashion. The planar NAr₂ ligand is tilted ($\varphi = 69.9(2)^\circ$) from the σ -ligand plane of the titanocene allowing the N lone pair to point toward the central carbon atom of the carbodiimide. The C24-N2 bond (1.264(6) Å) is considerably elongated compared to C24-N3 (1.189(6) Å), consistent with Lewis acidic activation of the former by the d⁰ Ti cation. Surprisingly, the Ti-amido bond is marginally longer than in **1b** ($\Delta d = 0.026(4)$ Å).

In the solid state, complex **2b'** features a planar four-membered TiNCN metallacycle with Ti-N distances of 2.0722(15) and 2.0790(13) Å; these values are expectedly lower than those for the neutral Ti(III) guanidinate complex previously reported by Rosenthal (2.196(2) and 2.193(1) Å).^[24] In solution, the ¹⁵N NMR



Scheme 6. Reaction of **1b** with diisopropylcarbodiimide (DIC).

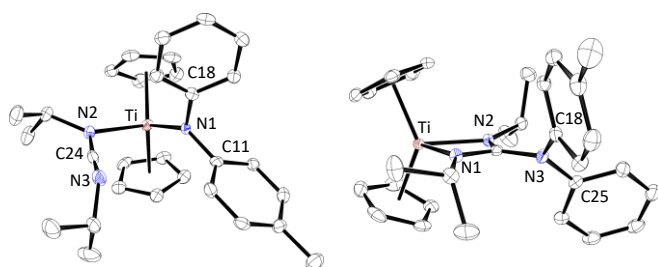


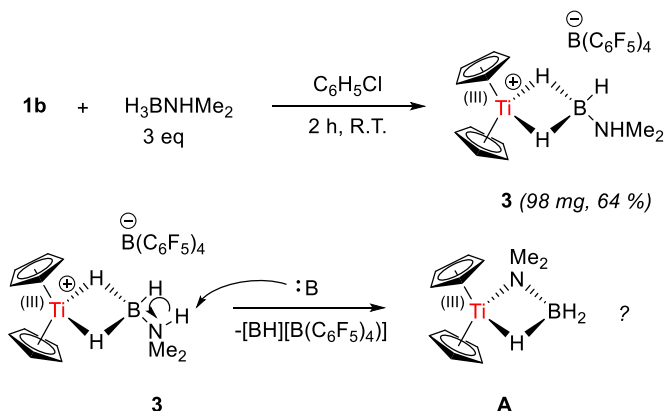
Figure 6. ORTEP views of complexes **2b** (left) and **2b'** (right). H atoms and the $\text{B}(\text{C}_6\text{F}_5)_4^-$ anion are omitted for clarity.

signal of the amido-derived nitrogen (observed indirectly by ¹H-¹⁵H HMBC) is considerably more shielded than in **1b** (-289 vs -33 ppm), while N1 and N2 both resonate at -200 ppm. The reaction of **1b** with DIC highlights the potential of amidotitanocene cations for the cooperative activation of organic molecules. Two other reactivity experiments suggested that they might also be active catalysts for a range of transformations, regardless of considerations as to their cooperative reactivity.

Additionally, reacting an excess of Et_3SiH with **1b** in $\text{C}_6\text{D}_5\text{Br}$ resulted in the formation of $\text{Ph}(p\text{-Tol})\text{NSiEt}_3$, as observed by ¹H NMR spectroscopy (Figure S60). The X-band EPR spectrum of the reaction mixture indicated that **1b** had been converted to a mixture of cationic Ti(III) species (Figure S61). This experiment prompted us to investigate the catalytic properties of **1a-c** in the dehydrocoupling of amines and silanes (vide infra).

In another experiment, we treated **1b** with 100 eq of dimethylamine-borane complex in $\text{C}_6\text{D}_5\text{Br}$, in the hope that dehydrogenation would occur.^[25] Indeed, titanocene-derived species are known to catalyze this transformation.^[26] The ¹¹B NMR spectrum showed no conversion to dehydrogenation products; however, the X-band EPR spectrum indicated that a Ti(III) complex had formed. We repeated the reaction under stoichiometric conditions in $\text{C}_6\text{H}_5\text{Cl}$: upon mixing the reagents, the

reaction mixture turned deep brown-red immediately, and gradually faded to pale brown. Complex **3** was eventually isolated as purple crystals in 64 % yield after workup and crystallization of the crude mixture (Scheme 7, top). GCMS analysis of the reaction mixture indicated the presence of 4-methyldiphenylamine and/or the corresponding hydrazine. To the best of our knowledge, **3** is the first example of structurally characterized Ti-(dimethylamine-borane) complex, and the second group 4 example.^[27] Importantly, it acts as an amine-borane dehydrogenation precatalyst (vide infra).



Scheme 7. Top: Reaction of **1b** with dimethylamine borane complex. Bottom: hypothetical synthesis of dehydrogenation catalyst **A** by deprotonation of complex **3**.

The X-ray structure of **3** (Figure 7, left) shows the presence of two independent molecules in the cell. Since both display similar geometrical features, we will only discuss one of them. It is interesting to compare the bond distances of **3** with those of **A** (a dehydrogenation catalyst reported by Manners and coworkers),^[26b] and free H_3BNHMe_2 .^[28] Intriguingly, **A** could be considered as the conjugate base of **3**, as suggested by Scheme 7 (vide infra).

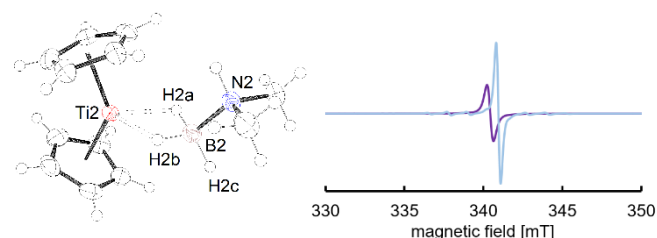


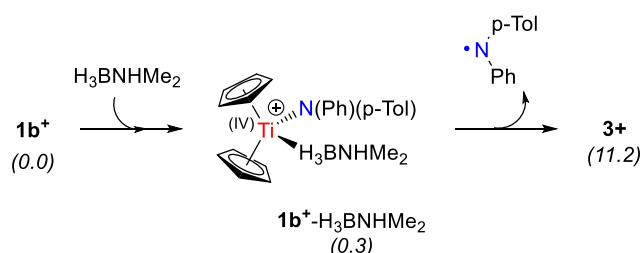
Figure 7. (left) ORTEP view of one of the independent molecules of complex **3**. The $\text{B}(\text{C}_6\text{F}_5)_4^-$ anion was omitted for clarity. (right) X-band EPR spectrum of **3** in $\text{C}_6\text{H}_5\text{Cl}$ (purple) and THF (blue) recorded at 294 K.

The Ti-B distance in **3** (2.419(3) Å) is noticeably shorter than in **A** (2.542(3) Å); it is actually just within the sum of covalent radii for both atoms (2.44 ± 0.11 Å).^[9] Interestingly, N-B distances are very similar for all three compounds (**3**: 1.582(4) Å; **A**: 1.586(3) Å; H_3BNHMe_2 : 1.596(1) Å) despite the different environments.

The X-band EPR spectrum of **3** in $\text{C}_6\text{H}_5\text{Cl}$ (Figure 7, right, purple) only shows one absorption at $g = 1.998$. In THF (Figure 7, right, blue), formation of $[\text{Cp}_2\text{Ti}(\text{THF})_2][\text{B}(\text{C}_6\text{F}_5)_4]$ is observed ($g = 1.973$, $A^{(47/49\text{Ti})} = 11.5 \times 10^{-4} \text{ cm}^{-1}$), along with free H_3BNHMe_2 (observed by ¹H and ¹¹B NMR spectroscopy, Figures S49 and S50). This

behavior is consistent with the view of H_3BNHMe_2 acting as a moderately donating neutral ligand towards Ti.

In order to elucidate the mechanism of formation of **3** we reacted **1b** with 1 eq of H_3BNHMe_2 in CD_2Cl_2 below 235 K and we analyzed the mixture by NMR spectroscopy. The $^{11}\text{B}\{^1\text{H}\}$ NMR spectrum shows the presence of the $\text{B}(\text{C}_6\text{F}_5)_4^-$ anion, and a broad signal is detected at ~ -9 ppm, but the signal of H_3BNHMe_2 was not visible anymore. This suggests the formation of an intermediate Lewis adduct between **1b** and H_3BNHMe_2 (Scheme 8). Consistent with this hypothesis, the ^1H NMR spectrum features a new Cp signal at 6.08 ppm and a broad signal at -0.69 ppm integrating for 3 protons, which we assign to the B-H protons of the **1b**- H_3BNHMe_2 adduct (Figure S63). Monitoring the reaction by UV-vis spectroscopy ($\text{C}_6\text{H}_5\text{Br}$, room temperature) revealed an isosbestic point at 312 nm, consistent with the formation of a single intermediate on the path from **1b** to **3** (Figure S64). Finally, we computed the energies of **1b** $^+$, **3** $^+$ and **1b**- H_3BNHMe_2 $^+$ by DFT and found that the formation of the latter is only slightly endergonic ($0.3 \text{ kcal}\cdot\text{mol}^{-1}$).



Scheme 8. Computed relative free energies ($\text{kcal}\cdot\text{mol}^{-1}$) for the formation of **3** in $\text{C}_6\text{H}_5\text{Br}$.

We analyzed the bonding situation in **3** with Bader's Quantum Theory of Atoms in molecules (QTAIM),^[29] and a plot of Non-Covalent Interactions (NCI)(Figure 8).^[30]

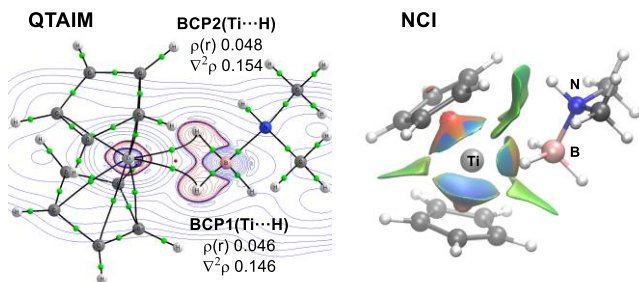


Figure 8. (Left) contour plot of the Laplacian of the electron density of **3** $^+$ with relevant bond paths (black lines) and bond critical points (green dots). (right) NCI plot of **3** $^+$ (blue: strong attraction; green: very weak interaction; red: strong repulsion).

The values of the electronic density ($\rho = 0.048$ and 0.046 a.u.) and its Laplacian ($\nabla^2\rho = 0.154$ and 0.146 a.u.) at the bond critical points between Ti and H confirm that the Ti center in **3** is stabilized by agnostic-like interactions with the borane moiety.^[31] No bond critical point was found between Ti and B, thus indicating that the relatively short Ti-B distance of $2.542(3) \text{ \AA}$ is actually due to electrostatic attraction between Cp_2Ti^+ and H_3BNHMe_2 . This interaction is possibly strengthened by dispersion interactions between the Cp and H_3BNHMe_2 ligands, as evidenced by the NCI plot.

Catalytic hydrogenation

Our initial interest in the catalytic properties of **1a-c** originated from results obtained previously with Zr species.^[2a] In line with the catalytic hydrogenation activity of **I-II**, we found that **1a-c** efficiently catalyze the hydrogenation of olefins and alkynes under mild conditions (room temperature, atmospheric pressure)(Table 2).^[32]

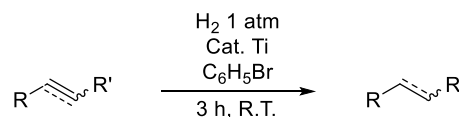


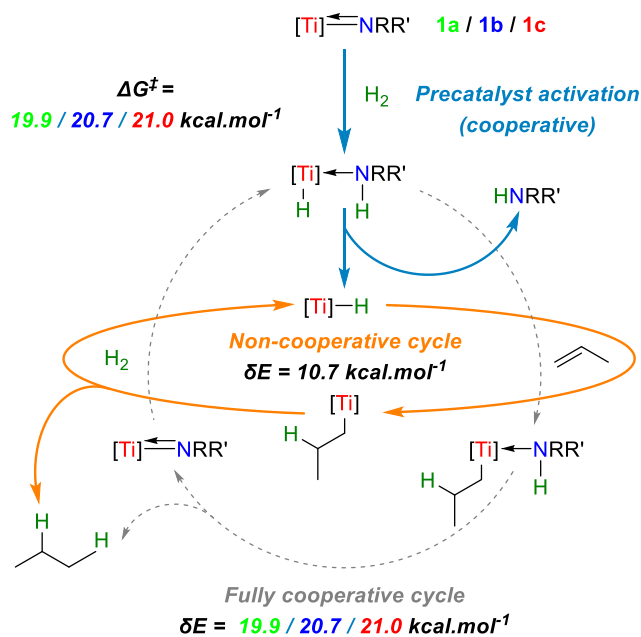
Table 2. Catalytic hydrogenation with **1a-c**.^[a]

Entry	Catalyst (loading) ^[a]	Substrate	Product	NMR Yield (%) ^[b]
1	1a/1b/1c (2 %)			97/87/79
2	1a/1b/1c (2 %)			69/74/55
3	1a/1b/1c (4 %)			95/53/14
4	1a/1b/1c (4 %)			4/3/traces
5	1a/1b/1c (4 %)			12/8/4 ^[c]

[a]: reagents and conditions: $\text{C}_6\text{H}_5\text{Br}$ 1 mL, substrate 0.960 M, trimethoxybenzene (TMB) 0.0480 M, catalyst 0.0192 M (entries 1 and 2); substrate 0.480 M, TMB 0.0480 M, catalyst 0.0192 M (entries 3-5); [b]: NMR yield (average of two runs) determined by integration versus TMB standard; [c]: conversion determined by integration vs starting material.

Compared to amido- and phosphidozirconocene cations **I-II**, complexes **1a-c** are somewhat less active,^[33] but also more selective: styrene was hydrogenated to ethylbenzene exclusively, whilst in the case of **I-II**, 1,4- and 2,4-diphenylbutane were obtained as minor C-C coupling products. The limitations of the Ti and Zr systems are the same: electron-poor alkenes (e.g. pentafluorostyrene, entry 4) and imines (e.g. N-benzylideneaniline, entry 5) gave very low conversions.

A remarkable feature of these hydrogenation results is the influence of the amido ligand on reaction kinetics. For instance, **1a** catalyzes the hydrogenation of diphenylacetylene much more efficiently than **1b** and **1c** (entry 3). The same trends were observed, albeit less dramatically, for all tested substrates. A similar influence of the amido/phosphide ligands was also noted for Zr complexes **I-II**; therefore, we had previously proposed a cooperative mechanism in which H_2 is activated by 1,2-addition at the M-E bond ($\text{E} = \text{N}, \text{P}$), thus generating a cationic d^0 metal hydride and a secondary amine (or phosphine). This step would be followed by olefin (or alkyne) insertion into the M-H bond, and protonolysis of the M-C bond by the coordinated amine/phosphine (Scheme 9, dashed arrows).^[2a] In order to probe our hypothesis, we conducted DFT calculations on the hydrogenation of propene by **1a-c** $^+$ in $\text{C}_6\text{H}_5\text{Br}$ (SMD model, see the Supporting Information for computational details). We found that this cooperative mechanism is indeed kinetically feasible, as evidenced by the $\sim 20 \text{ kcal}\cdot\text{mol}^{-1}$ computed energetic span (δE , Scheme 9).^[34]



Scheme 9. Simplified mechanisms computed by DFT for the catalytic hydrogenation of unsaturated substrates with **1a-c** ($[M] = \text{Cp}_2\text{Ti}^+$; $E = \text{N}$) For clarity, only propene 1,2-insertion is shown. Energy values refer to the computed free energies for **1a-c**.

Nevertheless, it became apparent that another mechanism is more likely, in which the amine ligand is expelled permanently from the coordination sphere and the M-C protonolysis step is effected by H_2 alone.^[35] In this mechanism, the cooperative 1,2-addition of H_2 across the Ti-N bond is merely a precatalyst activation step which lies outside of the main catalytic cycle. Once this $\sim 20 \text{ kcal.mol}^{-1}$ barrier is overcome ($\mathbf{1a}^+ < \mathbf{1b}^+ < \mathbf{1c}^+$), the energetic span of the non-cooperative cycle is much lower ($10.7 \text{ kcal.mol}^{-1}$). Obviously, the value of δE is the same for all three complexes: this suggests that the observed differences between **1a-c** are due to incomplete pre-catalyst activation, and thus different concentrations of the active catalyst (Cp_2TiH^+).^[36]

In order to better understand the factors governing the energy barrier of the catalyst activation step, we applied the Activation Strain Model (ASM) to **1a** and **1c**, which display the lowest and highest transition states, respectively (Figure 9). The energy decomposition scheme embedded in the ASM splits the activation energy in two terms (ΔE_{strain} and ΔE_{int}) which represent the energy required for distorting the reactants, and the interaction energy between them. This scheme enables the deconvolution of steric and electronic effects, and the ex-ante identification of better (pre)catalyst based on computational evidence.^[37]

The activation strain diagrams shown in Figure 9 reveal that the energy barrier for H_2 activation is mainly determined by ΔE_{strain} , which undergoes a $\sim 15 \text{ kcal.mol}^{-1}$ increase, whilst ΔE_{int} only decreases by $\sim 7 \text{ kcal.mol}^{-1}$.^[38] The reason for the increase in ΔE_{strain} is that, as the reactants progress towards the transition state, the rotation of the amido ligand causes severe distortion of the Ti complex. This suggests that less sterically congested precatalysts should be more easily activated, and indeed the activation barrier of the putative $\text{Cp}_2\text{Ti}(\text{NPhMe})^+$ cation (**1d**⁺) was computed at $18.1 \text{ kcal.mol}^{-1}$. By contrast, a $26.4 \text{ kcal.mol}^{-1}$ barrier was computed for $\text{Cp}_2\text{Ti}(\text{carbazole})^+$ (**1e**⁺). Thus, the ASM provides useful suggestions to control precatalyst activation.

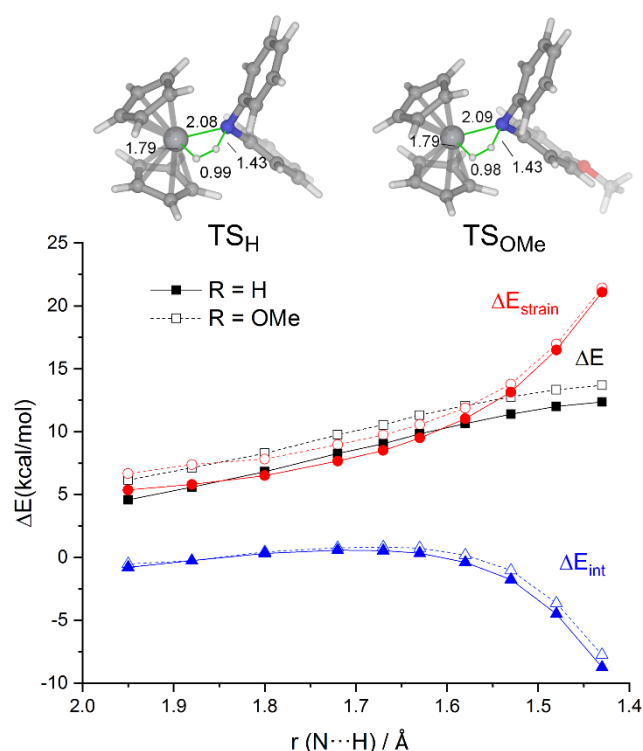


Figure 9. Comparative activation strain diagrams of the precatalyst activation step by **1a**⁺ with $R=\text{H}$ (solid lines) and $R=\text{OMe}$ (dashed lines) along the reaction coordinate projected onto the forming N...H bond length.

Catalytic dehydrogenation

Catalytic dehydrocoupling of amines and silanes (Scheme 10, next page) can be effected by a wide range of elements across the periodic table.^[39] To date, the most active catalyst for this reaction is a cationic cyclometallated N-heterocyclic carbene Pt complex reported by Conejero and coworkers, which couples electron-rich amines and primary/secondary silanes with high efficiency (TON up to 10^5).^[40] Other prominent homogeneous catalysts include Ba,^[41] Zn,^[42] Ru,^[43] Rh,^[44] Ir,^[45] as well as B- and P-based main group Lewis acids.^[46] Turnover numbers for these systems never exceed 1000 (400 for non-precious metals).

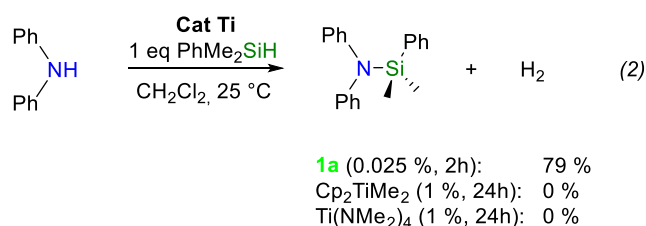
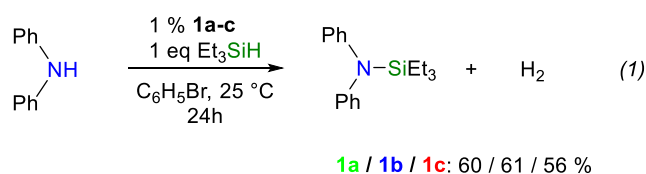
Heterogeneous catalyst based on precious metals such as Pd and Au have also been reported (TON up to 3.10^4 for Pd/graphene).^[47] Therefore, although highly efficient systems are known, they are based on precious metals, which makes the discovery of catalysts based on earth-abundant elements desirable.

Using **1a** as a catalyst, we initially screened the dehydrocoupling of Ph_2NH with primary, secondary and tertiary silanes (0.025% loading, CH_2Cl_2 , 25°C , Scheme 10). Surprisingly, PhSiH_3 , PhMeSiH_2 , Ph_2SiH_2 , PhMe_2SiH and Ph_2MeSiH all gave excellent results (NMR yield: 76-99%; TON: 1520-3960). In the case of PhSiH_3 , the reaction was scaled-up and we isolated $\text{Ph}_2\text{NSiH}_2\text{Ph}$ in 62% yield (1.71 g) after Kugelrohr distillation. On the other hand, the reaction with Ph_3SiH and Et_3SiH was comparatively sluggish, and higher loadings of **1a** (1-1.5%) had to be used for the reaction to proceed at acceptable rates.

Other amines could be coupled as well. Using Et_3SiH as a poorly reactive benchmark (1% loading, $\text{C}_6\text{H}_5\text{Br}$, 25°C), we were able to establish that electron-donating substituents on the aryl ring of PhArNH ($\text{Ar} = \text{Ph}$, *p*-Tol, *o*-An) further diminish reaction rates

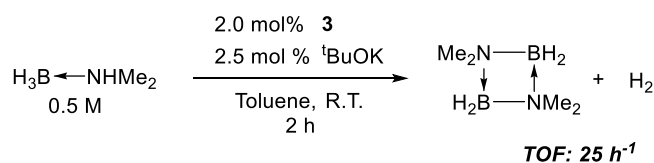
(TON after 24 h: 60, 47 and 40, respectively). With reactive silanes (PhMeSiH₂, Ph₂SiH₂, Ph₂MeSiH and Ph₂MeSiH; 0.25-0.5 % loading, CH₂Cl₂, 25 °C), N-methylaniline, mesitylamine (MesNH₂), indole and carbazole can be coupled in 58-98 % NMR yield and 176-392 TONs. The coupling product of carbazole and PhMe₂SiH was isolated in 95 % yield (1.43 g) after precipitation from a scaled-up experiment. On the other hand, PhNH₂ reacted poorly, whilst pyrrole,^tBuNH₂ and morpholine gave no conversion to aminosilanes (see the supporting information, Table S1).

We compared the catalytic performance of **1a** versus **1b** and **1c** on the one hand (Scheme 11, eq 1), and Cp₂TiMe₂ and Ti(NMe₂)₄ on the other (Scheme 11, eq 2). Unsurprisingly, **1a-c** display almost identical results: this strongly suggests that the amido ligand is replaced after one turnover. By contrast, Cp₂TiMe₂ and Ti(NMe₂)₄ were completely inactive under our conditions. These observations highlight the specificity of the outstanding catalytic activity of **1a-c** compared to common Ti complexes.^[48] We are currently investigating the mechanism by which this system operates, experimentally and computationally.



Scheme 11. Comparison of catalyst performance in the dehydrocoupling of amines and silanes.

Finally, we tested the catalytic properties of **3** in the dehydrogenation of H₃BNHMe₂ (Scheme 12). The reaction of **3**, potassium tert-butoxide and H₃BNHMe₂ (toluene, room temperature) resulted in immediate gas evolution. Monitoring the mixture by ¹¹B NMR spectroscopy revealed complete conversion of H₃BNHMe₂ to the dimethylaminoborane dimer after 2 h (Figure S128). No conversion was observed in the absence of base or **3** (Figure S129). Other bases, such as NEt₃ and potassium hexamethyldisilazane (KHMDs) were also effective (Figure S130).^[49] Interestingly, against our expectation that reaction of **3** with KO^tBu would yield the known dehydrogenation catalyst **A** (Scheme 7), we obtained a complex mixture instead (Figures S65-68). Detailed investigations into the mechanism of amine-borane dehydrogenation by **3** and the nature of the active catalyst are thus warranted.^[50]



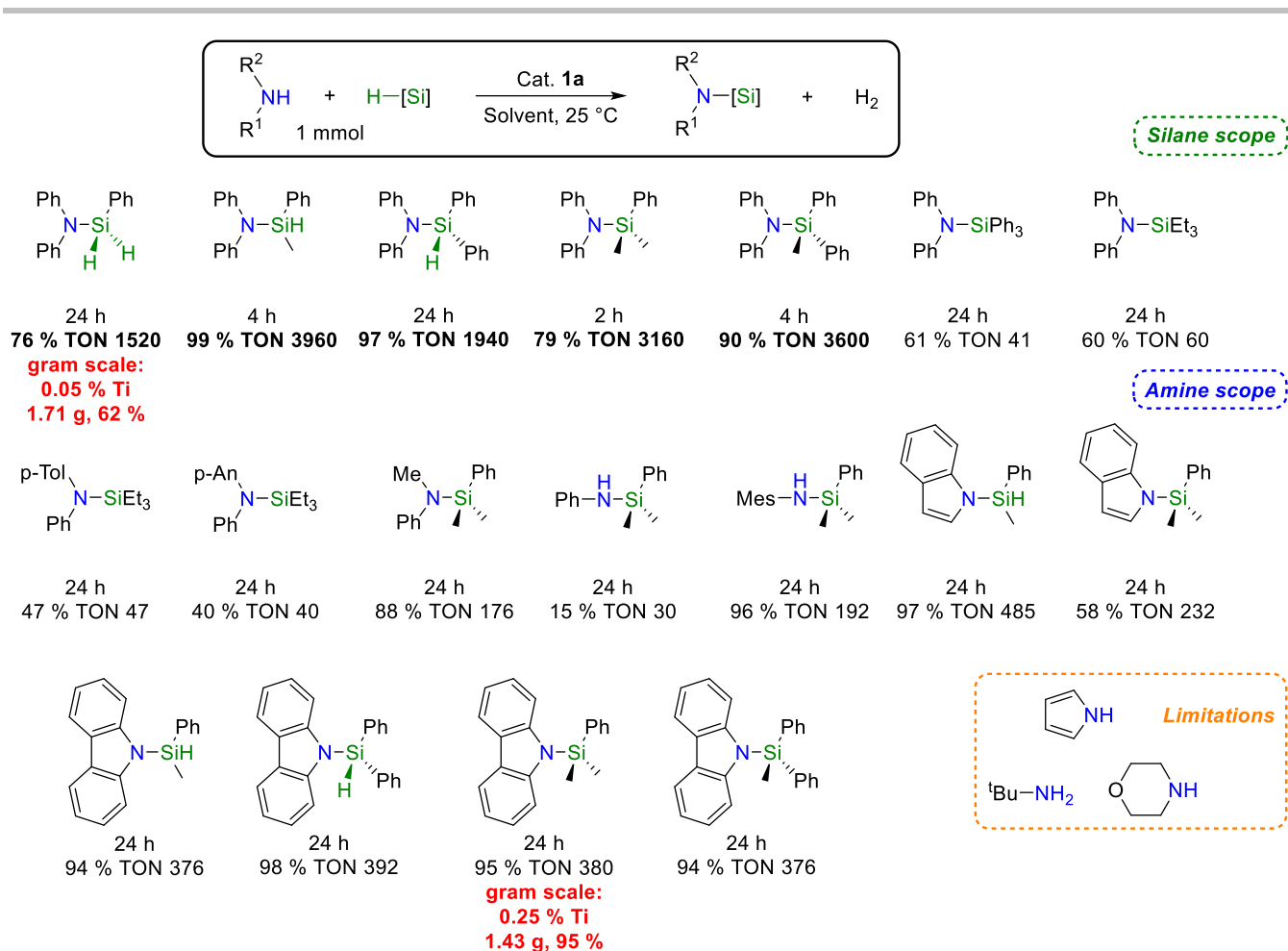
Scheme 12. Catalytic dimethylamine-borane dehydrogenation with **3**.

Conclusion

Amidotitanocene cations such as **1a-c** display an unusual Ti-N bonding situation with inverted σ and π bond strengths. This feature is likely related to the ease with which they undergo controlled release of aminyl radicals upon chemical or photochemical activation. Moreover, **1a-c** display high reactivity towards E-H bonds (E = H, B, Si), which may be harnessed in catalytic transformations of such bonds:

- Firstly, as evidenced by DFT calculations, the activation of H₂ proceeds by 1,2-addition to the Ti-N bond, enabled by the polar nature of the latter. Facile hydrogenation of unsaturated hydrocarbons under mild conditions ensues. Hence, **1a-c** may be viewed as "Cp₂TiH⁺" precatalysts.
- Secondly, **1a-c** achieve class-leading catalytic performances (for a non-precious metal) in the dehydrocoupling of amines and silanes, which warrants further investigations into the mechanism of this transformation.
- Thirdly, reaction with the dimethylamine-borane complex yields a rare d¹ Ti cation stabilized by agnostic-like interactions with the borane moiety (**3**), which doubles up as a precatalyst for amine-borane dehydrogenation.

We are currently expanding the family of amidotitanocene cations in order to generate and control synthetically useful aminyl radicals. We are also exploring the use of **1a-c** as two-way catalysts for hydrogen storage / release strategies.



Scheme 10. Catalytic amine silane dehydrocoupling with **1a**. Reagents and conditions: CH_2Cl_2 1.5 mL (except for Et_3SiH tests: $\text{C}_6\text{H}_5\text{Br}$ 1.5 mL), amine and silane 0.67 M, internal standard (mesitylene) 0.073 M, complex **1a** (0.025–1.5 %), NMR yield (average of two runs) determined by integration versus mesitylene standard. Conditions for the gram scale experiments: see the Supporting Information.

Acknowledgements

The authors would like to thank Prof Gerhard Erker for numerous discussions over the years about group IV amides and phosphides. We are deeply indebted to Prof Ewen Bodio and Dr Christine Goze for sharing their financial resources. We also thank Prof Marek Kubicki and Dr Diego Andrada for fruitful discussions about the electronic structure of Titanium amides, and EDA-NOCV analysis, respectively. Dr Natacha Goutay (COHESIVES) kindly loaned the 395 nm LED flood lamp. We also thank Mr Marcel Soustelle and Ms Tiffany Régner (PACSMUB) for elemental analyses. Financial support from CNRS, UB, ANR (ALCATRAS, ANR-16-CE07-0001-01), Conseil Régional de Bourgogne Franche-Comté (PhosFerTiMn, PARI CDEA), FEDER and the PIA-excellence ISITEBFC program (COMICS) is gratefully acknowledged. Calculations were performed using HPC resources from DSICUB (Université de Bourgogne). This work was granted access to the HPC resources of CINES under the allocation A0090807259 made by GENCI.

Keywords: Titanium • Catalysis • Hydrogen • Energy Decomposition Analysis • Activation Strain Model

Experimental Part

All reactions were carried out under Ar using conventional Schlenk techniques or in an Ar glovebox. The identity and purity of the compounds were established using elemental analysis, high-resolution mass spectrometry (ESI-MS), X-ray diffraction analysis, NMR, EPR, IR and UV-vis spectroscopies. The H content of $\text{B}(\text{C}_6\text{F}_5)_4^-$ containing compounds was found to be unreliable due to overlap between the peak of H_2O and that of the fluorine-containing effluent, as shown on Figure S1. For further details, see the supporting information.

General procedure for the synthesis of **1a-c**

Complexes **1a-c** can typically be prepared on a 1 mmol scale using the following procedure: In an Ar glovebox, three solutions were prepared, each containing 1 eq of reagent in $\text{C}_6\text{H}_5\text{Br}$: solution A (freshly prepared Cp_2TiMe_2 , 2 mL), solution B ($[\text{Ph}_3\text{C}][\text{B}(\text{C}_6\text{F}_5)_4]$, 4 mL), and solution C (amine, 2 mL). Solution A was stirred magnetically and solutions B, then C, were added dropwise with a pipette. The effervescing reaction mixture was stirred for 5 min, before being added to 100 mL of pentane under vigorous agitation. The precipitated solid was filtered over a sintered glass frit and dried in the glovebox. Complexes **1a-c** were obtained as dark green powder.

(1a) Elemental Analysis: % Calcd for $\text{C}_{46}\text{H}_{20}\text{BF}_5\text{NTi}$: C, 53.89; H, 1.97; N, 1.37. Found: C, 54.51; H, 2.24; N, 1.44. UV-vis (CH_2Cl_2 , 0.1 mm cell): $\lambda_{\text{max}} = 395 \text{ nm}$ ($8900 \text{ M}^{-1}\cdot\text{cm}^{-1}$). IR (ATR): 3120 (w), 1642 (w), 1512 (m),

1456 (s), 1383 (w), 1370 (w), 1273 (w), 1188 (w), 1085 (s), 1023 (w), 1014 (w), 973 (s), 930 (w), 906 (w), 860 (w), 843 (w), 824 (m), 821 (m), 770 (m), 763 (m), 753 (m), 726 (w), 704 (m), 696 (m), 683 (m), 663 (m), 610 (w), 602 (w), 573 (w), 541 (w), 503 (w), 474 (w), 441 (w). ¹H NMR (600 MHz, 298 K, C₆D₅Br): δ = 7.12 (m, 4H, *m* of NPh), 6.99 (m, 2H, *p* of NPh), 6.14 (s, 10H, Cp), 5.75 (m, 4H, *o* of NPh). ¹H-¹H COSY (600 MHz, 298 K, C₆D₅Br)[selected cross-peaks]: δ = 7.12 / 6.99 (*m* of NPh / *p* of NPh), 7.12 / 5.75 (*m* of Ph / *o* of NPh), 6.99 / 7.12 (*p* of NPh / *m* of NPh), 5.75 / 7.12 (*o* of Ph / *m* of NPh). ¹H-¹³C HMBC (600 MHz / 151 MHz, 298 K, C₆D₅Br)[selected cross-peaks]: δ = 7.12 / 156.0 (*m* of NPh / *i* of NPh), 7.12 / 131.4 (*m* of NPh / *m* of NPh), 6.99 / 117.7 (*p* of NPh / *o* of NPh), 5.75 / 128.8 (*o* of NPh / *p* of NPh), 5.75 / 117.7 (*o* of NPh / *o* of NPh). ¹H-¹⁵N HMBC (600 MHz / 61 MHz, 298 K, C₆D₅Br): δ = 5.75 / -35 (*o* of NPh / N). ¹³C{¹H} NMR (151 MHz, 298 K, C₆D₅Br): δ = 156.0 (s, *i* of NPh), 148.6 (dm, ¹J_{CF} = 240 Hz, *o* of C₆F₅), 138.3 (dm, ¹J_{CF} = 240 Hz, *p* of C₆F₅), 136.5 (dm, ¹J_{CF} = 240 Hz, *m* of C₆F₅), 131.4 (s, *m* of NPh), 128.8 (s, *p* of NPh), 124.5 (bs, BC), 122.5 (s, Cp), 117.7 (s, *o* of NPh). ¹¹B{¹H} NMR (194 MHz, 298 K, C₆D₅Br): δ = -16.1 (ν_{1/2} = 22 Hz). ¹⁹F{¹H} NMR (565 MHz, 298 K, C₆D₅Br): δ = -131.6 (br s, 8F, *o* of C₆F₅), -161.6 (m, 4F, *p* of C₆F₅), -165.5 (br s, 8F, *m* of C₆F₅).

(1b) Elemental analysis % Calcd for C₄₇H₂₂BF₂₀N₃Ti: C, 54.31; H, 2.13; N, 1.35. Found: C, 54.14; H, 0.91; N, 0.48. UV-vis (CH₂Cl₂, 0.1 mm cell): λ_{max} = 400 nm (11100 M⁻¹.cm⁻¹). IR (ATR): 1642 (m), 1511 (s), 1456 (s), 1410 (m), 1374 (w), 1371 (m), 1272 (m), 1084 (s), 1014 (w), 973 (s), 922 (w), 905 (w), 885 (w), 867 (w), 857 (w), 835 (m), 829 (m), 821 (s), 811 (m), 787 (m), 770 (m), 751 (m), 727 (m), 699 (m), 683 (m), 663 (s), 632 (m), 610 (m), 602 (m), 573 (m), 547 (w), 539 (w), 507 (m), 474 (m), 439 (m). ¹H NMR (600 MHz, 298 K, C₆D₅Br): δ = 7.04 (m, 2H, *m* of NPh), 6.90 (m, 1H, *p* of NPh), 6.89-6.85 (m, 2H, *m* of NAr overlapping with NMR solvent signal), 6.11 (s, 10H, Cp), 5.55 (m, 2H, *o* of NPh), 5.54 (m, 2H, *o* of NAr), 2.15 (s, CH₃). ¹H-¹H COSY (600 MHz, 298 K, C₆D₅Br)[selected cross-peaks]: δ = 7.04 / 5.55 (*m* of NPh / *o* of NPh), 7.04 / 6.90 (*m* of NPh / *p* of NPh), 6.90 / 7.04 (*p* of NPh / *m* of NPh), 6.89-6.85 / 5.54 (*m* of NAr / *o* of NAr), 5.55 / 7.04 (*o* of NPh / *m* of NPh), 5.54 / 6.89-6.85 (*o* of NAr / *m* of NAr). ¹H-¹³C HMBC (600 MHz / 151 MHz, 298 K, C₆D₅Br)[selected cross-peaks]: δ = 7.04 / 155.8 (*m* of NPh / *i* of NPh), 6.90 / 118.4 (*p* of NPh / *o* of NPh), 6.89-6.85 / 152.4 (*m* of NAr / *i* of NAr), 6.89-6.85 / 132.7 (*m* of NAr / *m* of NAr), 6.89-6.85 / 20.9 (*m* of NAr / CH₃), 5.55 / 128.3 (*o* of NPh / *p* of NPh), 5.55 / 118.4 (*o* of NPh / *o* of NPh), 5.54 / 140.4 (*o* of NAr / *p* of NAr), 5.54 / 116.1 (*o* of NAr / *o* of NAr), 2.15 / 140.4 (CH₃ / *p* of NAr), 2.15 / 132.7 (CH₃ / *m* of NAr). ¹H-¹⁵N HMBC (600 MHz / 61 MHz, 298 K, C₆D₅Br): δ = 5.55 / -33 (*o* of NPh / N), 5.54 / -33 (*o* of NAr / N). ¹³C{¹H} NMR (151 MHz, 298 K, C₆D₅Br): δ = 155.8 (s, *i* of NPh), 152.4 (s, *i* of NAr), 148.5 (dm, ¹J_{CF} = 240 Hz, *o* of C₆F₅), 140.4 (s, *p* of NAr), 138.3 (dm, ¹J_{CF} = 240 Hz, *p* of C₆F₅), 136.5 (dm, ¹J_{CF} = 240 Hz, *m* of C₆F₅), 132.7 (s, *m* of NAr), 130.6 (s, *m* of NPh), 128.3 (s, *p* of NPh), 124.4 (bs, BC), 122.6 (s, Cp), 118.4 (s, *o* of NPh), 116.1 (s, *o* of NAr), 20.9 (s, CH₃). ¹¹B{¹H} NMR (194 MHz, 298 K, C₆D₅Br): δ = -16.2 (ν_{1/2} = 22 Hz). ¹⁹F{¹H} NMR (565 MHz, 298 K, C₆D₅Br): δ = -131.7 (br s, 8F, *o* of C₆F₅), -161.7 (m, 4F, *p* of C₆F₅), -165.6 (br s, 8F, *m* of C₆F₅).

(1c) Elemental analysis % Calcd for C₄₇H₂₂BF₂₀NOTi(C₅H₁₂)_{2.5}(C₆H₅Br)_{0.25}: C, 57.47; H, 4.21; N, 1.10. % Calcd for C₄₇H₂₂BF₂₀NOTi(C₅H₁₂)_{1.5}(C₆H₅Br)_{0.25}: C, 55.92; H, 3.46; N, 1.16. Found: C, 55.65; H, 0.51; N, 1.36. UV-vis (CH₂Cl₂, 0.1 mm cell): λ_{max} = 409 nm (8900 M⁻¹.cm⁻¹). IR (ATR): 3113 (b, w), 2958 (w), 2925 (w), 2860 (w), 1642 (m), 1593 (m), 1511 (s), 1497 (m), 1456 (s), 1374 (m), 1301 (m), 1272 (s), 1250 (s), 1196 (w), 1181 (w), 1160 (m), 1082 (s), 1023 (m), 972 (s), 906 (m), 822 (s), 773 (s), 768 (s), 755 (s), 739 (m), 726 (m), 692 (m), 682 (s), 660 (s), 624 (m), 609 (m), 601 (m), 572 (m), 552 (m), 527 (m), 474 (m), 457 (m), 448 (m), 430 (m). ¹H NMR (600 MHz, 298 K, C₆D₅Br): δ = 7.12 (m, 2H, *m* of NPh overlapping with bromobenzene signal), 6.99-6.93 (m, 1H, *p* of NPh overlapping with bromobenzene signal), 6.68 (m, 2H, *o* of NAr), 6.26 (s, 10H, Cp), 5.50 (m, 2H, *o* of NAr), 5.46 (m, 2H, *o* of NPh), 3.54 (s, CH₃). ¹H-¹H COSY (600 MHz, 298 K, C₆D₅Br)[selected cross-peaks]: δ = 7.12 / 5.46 (*m* of NPh / *o* of NPh), 7.12 / 6.99-6.93 (*m* of NPh / *p* of NPh), 6.99-6.93 / 7.12 (*p* of NPh / *m* of NPh), 6.68 / 5.50 (*m* of NAr / *o* of NAr), 5.50 / 6.68 (*o* of NAr / *m* of NAr), 5.46 / 7.12 (*o* of NPh / *m* of NPh). ¹H-¹³C HMBC (600 MHz / 151 MHz, 298 K, C₆D₅Br)[selected cross-peaks]: δ = 7.12 / 155.7 (*m* of NPh / *i* of NPh), 7.12 / 130.1 (*m* of NPh /

m of NPh), 7.12 / 119.1 (*m* of NPh / *o* of NPh), 6.99-6.93 / 130.1 (*p* of NPh / *m* of NPh), 6.99-6.93 / 119.1 (*p* of NPh / *o* of NPh), 6.68 / 161.3 (*m* of NAr / *p* of NAr), 6.68 / 147.2 (*m* of NAr / *i* of NAr), 6.68 / 117.5 (*m* of NAr / *m* of NAr), 5.50 / 161.3 (*o* of NAr / *p* of NAr), 5.50 / 117.5 (*o* of NAr / *m* of NAr), 5.46 / 128.3 (*o* of NPh / *p* of NPh), 5.46 / 119.1 (*o* of NPh / *o* of NPh), 3.54 / 161.3 (CH₃ / *p* of NAr). ¹H-¹⁵N HMBC (600 MHz / 61 MHz, 298 K, C₆D₅Br): δ = 5.50 / -30 (*o* of NAr / N), 5.54 / -30 (*o* of NPh / N).

¹³C{¹H} NMR (151 MHz, 298 K, C₆D₅Br): δ = 161.3 (s, *p* of NAr), 155.7 (s, *i* of NPh), 148.5 (dm, ¹J_{CF} = 240 Hz, *o* of C₆F₅), 147.2 (s, *i* of NAr), 138.4 (dm, ¹J_{CF} = 240 Hz, *p* of C₆F₅), 136.6 (dm, ¹J_{CF} = 240 Hz, *m* of C₆F₅), 130.1 (s, *m* of NPh), 128.3 (s, *p* of NPh), 124.4 (bs, BC), 123.0 (s, Cp), 119.1 (s, *o* of NPh), 117.5 (s, *m* of NAr), 117.2 (s, *o* of NAr), 55.4 (s, CH₃). ¹¹B{¹H} NMR (194 MHz, 298 K, C₆D₅Br): δ = -16.2 (ν_{1/2} = 22 Hz). ¹⁹F{¹H} NMR (565 MHz, 298 K, C₆D₅Br): δ = -131.7 (br s, 8F, *o* of C₆F₅), -161.7 (m, 4F, *p* of C₆F₅), -165.6 (br s, 8F, *m* of C₆F₅).

Complex 2b. In an Ar glovebox, complex **1b** (263 mg, 0.125 mmol) and di-isopropyl carbodiimide (47 mg, 0.50 mmol) were mixed in 2 mL of CH₂Cl₂. The reaction mixture turned brown-red immediately. A brown-red gum was precipitated by slow addition to 50 mL of pentane under vigorous agitation. Trituration in pentane (2x5 mL) followed by filtration over a sintered glass frit afforded complex **2b** as an unstable brown-red powder containing 0.15 eq of pentane as per ¹H NMR estimation (245 mg). The ¹H NMR spectrum of the material thus isolated contained significant amounts of **2b'**, which increased over time (Figure S51). Single crystals suitable for X-ray diffraction analysis were obtained by diffusion of cyclohexane into a chlorobenzene solution of **2b'** at room temperature.

Complex 2b'. In an Ar glovebox, complex **1b** (131 mg, 0.125 mmol) and di-isopropyl carbodiimide (97 mg, 0.77 mmol) were mixed in 2 mL of CH₂Cl₂. The reaction mixture turned red immediately. After transferring the mixture into a schlenk vessel, it was heated to 60 °C for 45 h. The cooled reaction mixture was transferred into the glovebox and precipitated by slow addition to 50 mL of pentane under vigorous agitation. After stirring for 10 min, the resulting solid was filtered over a sintered glass frit, and suspended twice in 10 mL of pentane. Compound **2b'** was obtained as a beige powder containing 1 eq of pentane as per ¹H NMR estimation (121 mg, 78 % yield). Elemental analysis was consistent with a solvent free formula, which could be due to partial desolvation during sample preparation, or incomplete combustion of pentane. **Elemental Analysis:** % calcd for C₅₄H₃₆BF₂₀N₃Ti: C, 55.65; H, 3.11; N, 3.61; Found: C, 55.22; H, 1.57; N, 3.73. UV-vis (CH₂Cl₂, 0.1 mm cell): λ_{max} = 262 nm (29900 M⁻¹.cm⁻¹); 352 nm (8900 M⁻¹.cm⁻¹). HRMS (Positive mode ESI, dichloromethane): m/z calcd. for C₃₀H₃₆N₃Ti [M]⁺ 486,23832; found 486,23679 (Δ = -3,147 ppm).

IR (ATR): 2976 (w), 1642 (w), 1511 (m), 1459 (s), 1422 (m), 1384 (w), 1366 (w), 1338 (w), 1273 (w), 1234 (w), 1198 (w), 1166 (w), 1085 (m), 977 (s), 819 (s), 774 (m), 769 (m), 756 (m), 726 (w), 704 (w), 702 (w), 692 (w), 683 (w), 661 (m), 610 (w), 602 (w), 572 (w), 533 (w), 510 (w), 484 (w), 439 (w), 430 (w). ¹H NMR (500 MHz, 298K, CD₂Cl₂): δ = 7.44 (m, 2H, *m* of NPh), 7.27 (m, 2H, *m* of NAr), 7.22 (m, 1H, *p* of NPh), 7.07 (m, 2H, *o* of NPh), 7.00 (m, 2H, *o* of NAr), 6.90 (s, 10H, Cp), 3.46 (hept, ³J_{HH} = 6.5 Hz, 2H, CH of ⁱPr), 2.38 (s, 3H, CH₃ of NAr), 0.88 (d, ³J_{HH} = 6.5 Hz, 12H, CH₃ of ⁱPr overlapping with pentane signal). ¹H-¹H COSY (600 MHz, 298 K, C₆D₅Br)[selected cross-peaks]: δ = 7.44 / 7.07 (*m* of NPh / *o* of NPh), 7.44 / 7.22 (*m* of NPh / *p* of NPh), 7.27 / 7.00 (*m* of NAr / *o* of NAr), 7.22 / 7.44 (*p* of NPh / *m* of NPh), 7.07 / 7.44 (*o* of NPh / *m* of NPh), 7.01 / 7.27 (*o* of NAr / *m* of NAr), 3.46 / 0.88 (CH of ⁱPr / CH₃ of ⁱPr), 0.88 / 3.46 (CH₃ of ⁱPr / CH of ⁱPr). ¹H-¹³C HMBC (500 MHz / 126 MHz, 298 K, CD₂Cl₂)[selected cross-peaks]: δ = 7.44 / 142.7 (*m* of NPh / *i* of NPh), 7.44 / 130.7 (*m* of NPh / *m* of NPh), 7.27 / 139.7 (*m* of NAr / *i* of NAr), 7.27 / 131.3, (*m* of NAr / *m* of NAr), 7.27 / 21.0 (*m* of NAr / CH₃ of NAr), 7.07 / 125.3 (*o* of NPh / *p* of NPh), 7.01 / 135.9 (*o* of NAr / *p* of NAr), 7.01 / 122.3 (*o* of NAr / *o* of NAr), 3.46 / 140.9 (CH₃ of ⁱPr / NCN), 3.46 / 24.9 (CH₃ of ⁱPr / CH₃ of ⁱPr), 2.38 / 135.9 (CH₃ of NAr / *p* of NAr), 2.38 / 131.3 (CH₃ of NAr / *m* of NAr), 0.88 / 51.5 (CH₃ of ⁱPr / CH of ⁱPr), 0.88 / 24.9 (CH₃ of ⁱPr / CH₃ of ⁱPr). ¹H-¹⁵N HMBC (600 MHz / 61 MHz, 298 K, C₆D₅Br): δ = 7.07 / -289 (*o* of NPh / NPhAr), 7.00 / -289 (*o* of NAr / NPhAr), 3.46 / -200 (CH of ⁱPr / NⁱPr), 0.88

/ -200 (CH₃ of ⁱPr / ^NPr). ¹³C NMR (126 MHz, 298K, CD₂Cl₂): δ = 148.5 (dm, ¹J_{CF} = 240 Hz, o of C₆F₅), 142.7 (s, *i* of NPh), 140.9 (s, NCN), 139.7 (s, *i* of NAr), 138.7 (dm, ¹J_{CF} = 240 Hz, *p* of C₆F₅), 136.6 (dm, ¹J_{CF} = 240 Hz, *m* of C₆F₅), 135.9 (s, *p* of NAr), 131.3 (s, *m* of NAr), 130.7 (s, *m* of NPh), 125.3 (s, *p* of NPh), 122.3 (s, o of NAr), 122.2 (s, Cp), 121.9 (s, o of NPh), 51.5 (s, CH of ⁱPr), 24.9 (s, CH₃ of ⁱPr), 21.0 (s, CH₃ of NAr). ¹¹B{¹H} NMR (160 MHz, 298 K, CD₂Cl₂): δ = -16.2 (ν_{1/2} = 22 Hz). ¹⁹F{¹H} NMR (470 MHz, 298 K, CD₂Cl₂): δ = -133.1 (br s, 8F, o of C₆F₅), -163.7 (m, 4F, *p* of C₆F₅), -167.5 (br s, 8F, *m* of C₆F₅).

Complex 3. In an Ar glovebox, complex **1b** (175 mg, 0.17 mmol) and the borane-dimethylamine complex (29.5 mg, 0.51 mmol) were mixed in 1.0 mL of C₆H₅Br. The reaction mixture was stirred for 30 minutes, during which it turned from dark red to violet. Addition of the reaction mixture to 50 mL of vigorously stirred pentane resulted in oil formation. The solvent was removed and 10 mL of pentane were added to the oil and allowed to stir for 5 minutes. Then the pentane was removed and the washing with pentane was repeated twice upon which a violet powder was obtained, which was shortly dried under vacuum, dissolved in about 0.8 ml of C₆H₅Cl and recrystallized by diffusion of cyclohexane (10 mL) at room temperature. Finally, purple crystals of **3** (98 mg, 64 %) were obtained. Single crystals suitable for X-ray diffraction analysis were obtained similarly on a small scale by diffusion of cyclohexane into a chlorobenzene solution of **3** at room temperature. Elemental Analysis: % calcd for C₃₆H₂₀B₂F₂₀NTi: C, 47.20; H, 2.20; N, 1.53; Found: C, 47.59; H, 0.19; N, 1.63. UV-vis (CH₂Cl₂, 0.1 mm cell): λ_{max} = 422 nm (1500 M⁻¹·cm⁻¹, shoulder). IR (ATR): 3304 (w), 3292 (w), 2456 (w), 2081 (b, w), 1643 (w), 1512 (m), 1456 (s), 1372 (m), 1371 (m), 1306 (w), 1272 (m), 1162 (w), 1082 (m), 973 (s), 922 (m), 895 (w), 812 (m), 773 (m), 769 (m), 727 (w), 683 (m), 661 (m), 610 (m), 602 (m), 573 (m), 599 (b, w), 474 (w). EPR (X-band, C₆H₅Cl, 294 K): g = 1.998. EPR (X-band, d₈-THF, 294 K): g = 1.973, A(^{47/49}Ti) = 11.5x10⁻⁴ cm⁻¹. ¹¹B{¹H} NMR (160 MHz, 298 K, d₈-THF): δ = -13.8 (bs, ν_{1/2} ≈ 60 Hz, BH₃), -16.9 (bs, ν_{1/2} ≈ 20 Hz, BC₆F₅). ¹¹B NMR (160 MHz, 298 K, d₈-THF): δ = -13.8 (bq, ¹J_{BH} = 90 Hz, BH₃), -16.9 (bs, ν_{1/2} ≈ 20 Hz, BC₆F₅). ¹⁹F{¹H} NMR (470 MHz, 298 K, d₈-THF): δ = -133.0 (br s, 8F, o of C₆F₅), -165.4 (m, 4F, *p* of C₆F₅), -168.8 (br s, 8F, *m* of C₆F₅).

Attempted syntheses and reactivity experiments

See the supporting information.

Olefin hydrogenation

A 0.048 M stock solution of trimethoxybenzene (TMB) was prepared in C₆H₅Br. The substrate (0.96 mmol or 0.48 mmol) and the catalyst (0.0192 mmol, 2 mol% or 4 %) were introduced in a 25 mL Schlenk tube and 1.0 mL of the TMB solution was added. The resulting solution was frozen, evacuated, and the vessel was backfilled with one atmosphere of H₂. After the indicated time, an aliquot of reaction mixture was collected and diluted with CDCl₃. The solution was analysed by ¹H NMR spectroscopy. Representative spectra are shown below (Figures S56-S60).

Cross-dehydrogenative coupling

All standard catalytic runs were performed in 10 mL crimp top vials containing a small octagonal stir bar. The quoted conversions are an average of at least two parallel runs. Solution of the standard (mesitylene) was prepared in a 25 mL volumetric flask in an Ar glovebox and stored in a freezer at -18 °C (in CH₂Cl₂) or at room temperature (in bromobenzene).

In an Ar glovebox, the silane (1 mmol) was weighed into a vial and 1 mL of stock solution of mesitylene was added (1 mL, 0.11 M in CH₂Cl₂ or bromobenzene, 0.11 mmol). Then the amine (1 mmol) and additional solvent to reach the total of 1.5 mL (taking into account the volume of the solution of the complex) were added. Finally, a solution of the complex **1** in either CH₂Cl₂ or bromobenzene (0.01M) was prepared and an aliquot was taken and added to the reaction mixture. For catalyst loadings lower than 0.05 mol% the solution was further diluted to increase the accuracy of the added volume. For catalyst loadings greater than 1 mol% the catalyst was weighed into the vial directly. After the addition, the vial was

quickly sealed with a crimp top, taken out of the glovebox and inserted into a thermostat or temperature regulated oil bath set to 25 °C. After the indicated time, the reaction vial was opened in an Ar glovebox and a sample for the NMR yield determination was prepared by diluting 0.15 mL of the reaction mixture with 0.50 mL of CDCl₃. NMR yield determination was performed on a Bruker AV600 spectrometer by ¹H NMR with d1 = 60 s, NS = 1, Acquisition time = 5 s. Experiments for the preparation of N,N,1-triphenylsilanamine, 9-(dimethyl(phenyl)silyl)-9H-carbazole and N,1,1-trimethyl-N,1-diphenylsilanamine on large scale were performed similarly. For details, see respective entries in the product characterization part. For structure confirmation the products of small scale runs were isolated from reactions showing high conversion by solvent evaporation (assumed quantitative yield with purity >95 %), and further purified by either filtration through an alumina plug (eluent petroleum ether:EtOAc, 9:1) or recrystallization from heptane when necessary.

Dimerization of borane-dimethylamine complex

In an Ar glovebox the borane dimethylamine complex (44.2 mg, 0.75 mmol) was weighed into a 10 mL crimp top vial containing a small octagonal stir bar. Complex **3** (13.8 mg, 2.0 mol%) was added and the solids were dissolved in 1.35 mL of toluene. Finally a stock solution of potassium *tert*-butoxide (0.125 M) in toluene was prepared and an aliquot (0.15 mL, 2.1 mg, 2.5 mol%) was measured and added to the reaction mixture. The vial was crimped and stirred inside a glovebox at ambient temperature. Samples for NMR analysis were taken through the crimp top by syringe (0.05 mL) and diluted with CDCl₃. Control experiments in a) absence of base, b) absence of complex **3** were performed similarly by omitting the addition of the corresponding reagent. NMR samples were prepared 2 hours after the start of the reaction.

Computational studies

See the supporting information for computational details and xyz files.

References

- [1] a) E. Y.-X. Chen and T. J. Marks, *Chem. Rev.* **2000**, *100*, 1391-1434; b) R. A. Collins, A. F. Russell and P. Mountford, *Applied Petrochemical Research* **2015**, *5*, 153-171; c) H. H. Brintzinger, D. Fischer, R. Mülhaupt, B. Rieger and R. M. Waymouth, *Angew. Chem. Int. Ed.* **1995**, *34*, 1143-1170.
- [2] a) A. T. Normand, C. G. Daniliuc, B. Wibbeling, G. Kehr, P. Le Gendre and G. Erker, *J. Am. Chem. Soc.* **2015**, *137*, 10796-10808; b) A. T. Normand, C. G. Daniliuc, G. Kehr, P. Le Gendre and G. Erker, *Dalton Trans.* **2016**, *45*, 3711-3714; c) A. T. Normand, C. G. Daniliuc, B. Wibbeling, G. Kehr, P. Le Gendre and G. Erker, *Chem. Eur. J.* **2016**, *22*, 4285-4293; d) A. T. Normand, Q. Bonnin, S. Brandès, P. Richard, P. Fleurat-Lessard, C. H. Devillers, C. Balan, P. Le Gendre, G. Kehr and G. Erker, *Chem. Eur. J.* **2019**, *25*, 2803-2815.
- [3] a) S. R. Flynn and D. F. Wass, *ACS Catalysis* **2013**, *3*, 2574-2581; b) B. Chatterjee, W.-C. Chang, S. Jena and C. Werlé, *ACS Catalysis* **2020**, *10*, 14024-14055.
- [4] the redox lability of titanocene-derived cations has long been known, see a) D. S. Breslow, N. R. Newburg, *J. Am. Chem. Soc.* **1957**, *79*, 5072-5073; b) D. S. Breslow, N. R. Newburg, *J. Am. Chem. Soc.* **1959**, *81*, 81-86; c) G. Henrici-Olivé, S. Olivé, *Angew. Chem. Int. Ed.* **1967**, *6*, 790-798.
- [5] a) R. Severin and S. Doye, *Chem. Soc. Rev.* **2007**, *36*, 1407-1420; b) M. Manßen and L. L. Schafer, *Chem. Soc. Rev.* **2020**, *49*, 6947-6994.
- [6] a) W. C. Danen and F. A. Neugebauer, *Angew. Chem. Int. Ed.* **1975**, *14*, 783-789; b) S. Z. Zard, *Chem. Soc. Rev.* **2008**, *37*, 1603-1618; c) T. Xiong and Q. Zhang, *Chem. Soc. Rev.* **2016**, *45*, 3069-3087; d) M. D. Kärkäs, *ACS Catalysis* **2017**, *7*, 4999-5022; e) P. Xiong and H.-C. Xu, *Acc. Chem. Res.* **2019**, *52*, 3339-3350; f) X.-Y. Yu, Q.-Q. Zhao, J. Chen, W.-J. Xiao and J.-R. Chen, *Acc. Chem. Res.* **2020**, *53*, 1066-1083.
- [7] J. Feldman and J. C. Calabrese, *J. Chem. Soc. Chem. Commun.* **1991**, 1042-1044.

- [8] a) J. W. Lauher and R. Hoffmann, *J. Am. Chem. Soc.* **1976**, *98*, 1729-1742; b) S. A. DiFranco, N. A. Maciulis, R. J. Staples, R. J. Batrice and A. L. Odum, *Inorg. Chem.* **2012**, *51*, 1187-1200; c) W. W. Lukens, M. R. Smith and R. A. Andersen, *J. Am. Chem. Soc.* **1996**, *118*, 1719-1728.
- [9] B. Cordero, V. Gomez, A. E. Platero-Prats, M. Reves, J. Echeverria, E. Cremades, F. Barragan and S. Alvarez, *Dalton Trans.* **2008**, 2832-2838.
- [10] M. Witanowski, L. Stefaniak and G. A. Webb, *Nitrogen NMR Spectroscopy*, in Annual Reports on NMR Spectroscopy, Vol. 25, Ed. G. A. Webb, Academic Press, **1993**, pp. 1-82.
- [11] S. Halbert, C. Copéret, C. Raynaud and O. Eisenstein, *J. Am. Chem. Soc.* **2016**, *138*, 2261-2272.
- [12] Y. Zheng, W. Zheng, J. Wang, H. Chang and D. Zhu, *J. Phys. Chem. A* **2018**, *122*, 2764-2780.
- [13] See Figures S11, S21 and S33 for the simulated spectra.
- [14] Moreover, the lifetime of $\cdot\text{NPh}_2$ is too short to observe it except by continuous UV-light irradiation of tetraphenylhydrazine under flow conditions, see: F. A. Neugebauer, S. Bamberger, *Angew. Chem. Int. Ed.* **1971**, *10*, 71-71.
- [15] K. Oberdorf, A. Hanft, J. Ramler, I. Krummenacher, F. M. Bickelhaupt, J. Poater and C. Lichtenberg, *Angew. Chem. Int. Ed.* **2021**, *60*, 6441-6445.
- [16] a) R. G. Hicks, *Angew. Chem. Int. Ed.* **2008**, *47*, 7393-7395; b) A. I. O. Suarez, V. Lyaskovskyy, J. N. H. Reek, J. I. van der Vlugt and B. de Bruin, *Angew. Chem. Int. Ed.* **2013**, *52*, 12510-12529; c) T. Büttner, J. Geier, G. Frison, J. Harmer, C. Calle, A. Schweiger, H. Schönberg and H. Grützmacher, *Science* **2005**, *307*, 235-238; d) D. Adhikari, S. Mossin, F. Basuli, J. C. Huffman, R. K. Szilagy, K. Meyer and D. J. Mindiola, *J. Am. Chem. Soc.* **2008**, *130*, 3676-3682; e) P. Maire, M. Königsmann, A. Sreekanth, J. Harmer, A. Schweiger and H. Grützmacher, *J. Am. Chem. Soc.* **2006**, *128*, 6578-6580; f) N. P. Mankad, W. E. Antholine, R. K. Szilagy and J. C. Peters, *J. Am. Chem. Soc.* **2009**, *131*, 3878-3880.
- [17] a) G. Frenking and F. M. Bickelhaupt, *The EDA Perspective of Chemical Bonding*, in The Chemical Bond, **2014**, pp. 121-157; b) P. Jerabek, P. Schwerdtfeger and G. Frenking, *J. Comput. Chem.* **2019**, *40*, 247-264; c) L. Zhao, M. Hermann, W. H. E. Schwarz and G. Frenking, *Nature Reviews Chemistry* **2019**, *3*, 48-63; d) L. Zhao, S. Pan, N. Holzmann, P. Schwerdtfeger and G. Frenking, *Chem. Rev.* **2019**, *119*, 8781-8845.
- [18] a) Y. Tulchinsky, M. A. Iron, M. Botoshansky and M. Gandelman, *Nat. Chem.* **2011**, *3*, 525-531; b) Y. Tulchinsky, S. Kozuch, P. Saha, A. Mauda, G. Nisnevich, M. Botoshansky, L. J. W. Shimon and M. Gandelman, *Chem. Eur. J.* **2015**, *21*, 7099-7110.
- [19] L. Rosenberg, *Coord. Chem. Rev.* **2012**, *256*, 606-626.
- [20] W. Su, S. Pan, X. Sun, S. Wang, L. Zhao, G. Frenking and C. Zhu, *Nature Communications* **2018**, *9*, 4997.
- [21] See the supporting information for the full table.
- [22] R. Tonner and G. Frenking, *Chem. Eur. J.* **2008**, *14*, 3260-3272.
- [23] C. Foroutan-Nejad, *Nature Communications* **2021**, *12*, 4037.
- [24] L. Becker, P. Arndt, H. Jiao, A. Spannenberg and U. Rosenthal, *Angew. Chem. Int. Ed.* **2013**, *52*, 11396-11400.
- [25] E. M. Leitao, T. Jurca and I. Manners, *Nat. Chem.* **2013**, *5*, 817-829.
- [26] a) A. M. Chapman and D. F. Wass, *Dalton Trans.* **2012**, *41*, 9067-9072; b) H. Helten, B. Dutta, J. R. Vance, M. E. Sloan, M. F. Haddow, S. Sproules, D. Collison, G. R. Whittell, G. C. Lloyd-Jones and I. Manners, *Angew. Chem. Int. Ed.* **2013**, *52*, 437-440; c) E. A. LaPierre, B. O. Patrick and I. Manners, *J. Am. Chem. Soc.* **2019**, *141*, 20009-20015.
- [27] O. J. Metters, S. R. Flynn, C. K. Dowds, H. A. Sparkes, I. Manners and D. F. Wass, *ACS Catalysis* **2016**, *6*, 6601-6611.
- [28] S. Aldridge, A. J. Downs, C. Y. Tang, S. Parsons, M. C. Clarke, R. D. L. Johnstone, H. E. Robertson, D. W. H. Rankin, D. A. Wann CCDC 732570: *Experimental Crystal Structure Determination*, **2009**, DOI: 10.5517/ccs99y.
- [29] a) R. Bader, *Atoms in molecules: a quantum theory*, Oxford University Press, **1994**; b) P. Lode and A. Popelier, *The QTAIM Perspective of Chemical Bonding*, in The Chemical Bond, Vol. 1, Eds.: G. Frenking and S. Shaik, **2014**, pp. 271-308; c) S. Shahbazian, *Chem. Eur. J.* **2018**, *24*, 5401-5405.
- [30] a) A. D. Becke and K. E. Edgecombe, *J. Chem. Phys.* **1990**, *92*, 5397-5403; b) B. Silvi and A. Savin, *Nature* **1994**, *371*, 683-686; c) Y. Grin, A. Shavin and B. Silvi, *The ELF Perspective of chemical bonding*, in The Chemical Bond, Vol. 1, Eds.: G. Frenking and S. Shaik, **2014**, pp. 345-382.
- [31] a) P. L. A. Popelier and G. Logothetis, *J. Organomet. Chem.* **1998**, *555*, 101-111; b) M. Lein, J. A. Harrison and A. J. Nielson, *Dalton Trans.* **2013**, *42*, 10939-10951.
- [32] a) Y. Tajima and E. Kunioka, *J. Org. Chem.* **1968**, *33*, 1689-1690; b) R. Stern, G. Hillion and L. Sajus, *Tetrahedron Lett.* **1969**, *10*, 1561-1566.
- [33] comparing the results between Zr and Ti is difficult since in the case of Zr, the pressure was 2.5 times higher, and catalyst loading was in general twice as low. See ref 2a.
- [34] a) C. Amatore and A. Jutand, *J. Organomet. Chem.* **1999**, *576*, 254-278; b) S. Kozuch and S. Shaik, *Acc. Chem. Res.* **2011**, *44*, 101-110.
- [35] T. C. Chung and J. Y. Dong, *J. Am. Chem. Soc.* **2001**, *123*, 4871-4876.
- [36] Titanocene hydrides are often implicated in catalytic reactions, see ref 4 and: a) J. E. Bercaw, R. H. Marvich, L. G. Bell, H. H. Brintzinger, *J. Am. Chem. Soc.* **1972**, *94*, 1219-1238; b) C. A. Willoughby, S. L. Buchwald, *J. Am. Chem. Soc.* **1992**, *114*, 7562-7564; c) C. A. Willoughby, S. L. Buchwald, *J. Am. Chem. Soc.* **1994**, *116*, 11703-11714; d) X. Verdagner, U. E. W. Lange, M. T. Reding, S. L. Buchwald, *J. Am. Chem. Soc.* **1996**, *118*, 6784-6785; e) T. D. Tilley, *Acc. Chem. Res.* **1993**, *26*, 22-29; f) R. Shu, L. Hao, J. F. Harrod, H.-G. Woo, E. Samuel, *J. Am. Chem. Soc.* **1998**, *120*, 12988-12989; g) E. A. LaPierre, B. O. Patrick, I. Manners, *J. Am. Chem. Soc.* **2019**, *141*, 20009-20015; h) E. Salvadori, M. Chiesa, A. Buonerba, A. Grassi, *Chem. Sci.* **2020**, *11*, 12436-12445.
- [37] a) I. Fernández and F. M. Bickelhaupt, *Chem. Soc. Rev.* **2014**, *43*, 4953-4967; b) E. D. Sosa Carrizo, F. M. Bickelhaupt and I. Fernández, *Chem. Eur. J.* **2015**, *21*, 14362-14369; c) F. M. Bickelhaupt and K. N. Houk, *Angew. Chem. Int. Ed.* **2017**, *56*, 10070-10086.
- [38] However, it should be noted that ΔE_{strain} determines the relative energies of the interacting fragments at low reaction coordinates, whilst ΔE_{int} prevails in the vicinity of the transition states ($r(\text{N}\cdots\text{H}) < 1.5 \text{ \AA}$).
- [39] a) K. Kuciński and G. Hreczycho, *ChemCatChem* **2017**, *9*, 1868-1885; b) M. B. Reuter, K. Hageman and R. Waterman, *Chem. Eur. J.* **2021**, *27*, 3251-3261.
- [40] P. Rios, M. Roselló-Merino, O. Rivada-Wheelaghan, J. Borge, J. López-Serrano and S. Conejero, *Chem. Commun.* **2018**, *54*, 619-622.
- [41] a) Y. Sarazin and J.-F. Carpentier, *Chem. Rev.* **2015**, *115*, 3564-3614; b) C. Bellini, V. Dorcet, J.-F. Carpentier, S. Tobisch and Y. Sarazin, *Chem. Eur. J.* **2016**, *22*, 4564-4583; c) C. Bellini, C. Orione, J.-F. Carpentier and Y. Sarazin, *Angew. Chem. Int. Ed.* **2016**, *55*, 3744-3748; d) C. Bellini, T. Roisnel, J.-F. Carpentier, S. Tobisch and Y. Sarazin, *Chem. Eur. J.* **2016**, *22*, 15733-15743.
- [42] T. Tsuchimoto, Y. Iketani and M. Sekine, *Chem. Eur. J.* **2012**, *18*, 9500-9504.
- [43] a) D. W. Robbins, T. A. Boebel and J. F. Hartwig, *J. Am. Chem. Soc.* **2010**, *132*, 4068-4069; b) C. D. F. Königs, M. F. Müller, N. Aiguabella, H. F. T. Klare and M. Oestreich, *Chem. Commun.* **2013**, *49*, 1506-1508.
- [44] a) H. Kono, I. Ojima, M. Matsumoto and Y. Nagai, *Org. Prep. Proc. Int.* **1973**, *5*, 135-139; b) S. Itagaki, K. Kamata, K. Yamaguchi and N. Mizuno, *Chem. Commun.* **2012**, *48*, 9269-9271.
- [45] a) T. A. Boebel and J. F. Hartwig, *J. Am. Chem. Soc.* **2008**, *130*, 7534-7535; b) Q. Li, M. Driess and J. F. Hartwig, *Angew. Chem. Int. Ed.* **2014**, *53*, 8471-8474.
- [46] M. Pérez, C. B. Caputo, R. Dobrovetsky and D. W. Stephan, *Proc. Nat. Ac. Sci.* **2014**, *111*, 10917-10921.
- [47] a) L. H. Sommer and J. D. Citron, *J. Org. Chem.* **1967**, *32*, 2470-2472; b) K. Taniguchi, S. Itagaki, K. Yamaguchi and N. Mizuno, *Angew. Chem. Int. Ed.* **2013**, *52*, 8420-8423; c) J. F. Blandez, I. Esteve-Adell, M. Alvaro and H. Garcia, *Cat. Sci. Technology* **2015**, *5*, 2167-2173; d) T. Mitsudome, T. Urayama, Z. Maeno, T. Mizugaki, K. Jitsukawa and K. Kaneda *Chem. Eur. J.* **2015**, *21*, 3202-3205.
- [48] Harrod and coworkers have previously shown that Cp_2TiMe_2 catalyzes the dehydrocoupling of ammonia or hydrazine with silanes: a) H. Q. Liu, J. F. Harrod, *Organometallics* **1992**, *11*, 822-827; b) J. He, H. Q. Liu, J. F. Harrod, R. Hynes, *Organometallics* **1994**, *13*, 336-343.
- [49] Reactions performed in $\text{C}_6\text{H}_5\text{Br}$ instead of toluene.
- [50] We thank an anonymous reviewer for suggesting this simple experiment. We note in passing that the superior performance of our system compared to **A** (TOF = 10.7 h^{-1} , see ref 26b) is consistent with the notion that **A** is not the active catalyst.